

## Numerical Analysis of External Supersonic Combustion of Hydrogen and Ethylene

J. R. Jones and F. C. Christo

Defence Science Technology Organisation - Weapons Systems Division  
 Weapons Propulsion Group, Edinburgh, South Australia 5111 AUSTRALIA

### Abstract

A numerical analysis using a CFD code specifically designed for hypersonic flows has been performed by modelling external supersonic combustion of hydrogen and ethylene fuels with hypersonic air flow at Mach 7.6. In comparison with the Coras-Paull [1,2] experimental data from the University of Queensland shock-tunnel, the results indicate good correlation of the relative pressure increase on fore (intake) and aft (thrust) surfaces due to fuel injection with and without combustion. For the geometry considered, air by itself results in an increase in the net drag force. With fuel injection and combustion the drag force increases further. Ethylene injection for several inflow conditions did not yield stable combustion, but only caused an increase in the drag force.

### Introduction

Hypersonic air-breathing propulsion, when fully realised, will revolutionise the paradigm within which both civil and military aviation operate. Although relatively simple in its theory, the high-speed environment and material limitations present significant challenges which require further investigation. One of the prevailing challenges in the design of hypersonic vehicles is reducing drag and generating sufficient thrust. The complexity of the challenge is augmented by the fact that the drag and thrust are usually interdependent parameters. Injection of additional fuel or oxidizer into a boundary layer has proven to reduce the effects of viscous drag through reduction of the velocity gradient and decrease in the local density of the flow in that region [1]. An initial research into external combustion was made by Johns Hopkins University back in the 1960's [3], [5]. Their conclusion was that although external burning could be a reasonable source of increasing lift and cancellation of drag, it was too inefficient to provide net thrust. With the recent advances in hypersonic research and technology, however, there is a renewed interest in the topic of external combustion. A better understanding of combustion in boundary layers could lead to further decreases in density, and reductions in Reynolds stresses. Since the Reynolds stresses are a strong function of the local density, and thus temperature, the shear stress along the wall would decrease [1]. From previous efforts, fuel injection along the wall has successfully reduced skin friction [6], but injection perpendicular to the flow has left it unaffected [7]. By creating a combustion zone on the aft surface of a vehicle, the induced pressure rise would not only minimize effects of separation and base drag, but could also provide a degree of forward thrust. The caveat is that in order for the fuel to initiate combustion, injection must occur in a region suitable for automatic ignition of the fuel [4].

The main objectives of this study are to validate the CFD solver and numerically quantify the pressure forces and external combustion characteristics over a ramp in a hypersonic flow. Comparison will then be made against ethylene for a variety of inflow conditions to quantify its performance against that of hydrogen.

### Experiment

The experimental results of external combustion of hydrogen from the University of Queensland were used to validate the CFD code. A complete review of the experimental analysis can be found in Ref. [1]. Only a brief summary is provided here for completeness of the presentation. The experiment was performed in the T4 shock tunnel at the University of Queensland. The physical model consisted of a 27.1° intake ramp with a total ramp length of 250 mm. At the apex of this ramp a sharp turn was made to a thrust surface which was inclined at 12.9° (numerical grid was inclined at 12.95°) relative to the horizontal [2]. Pressure transducers were located down the centreline of the ramp which had a constant width of 100 mm. Fuel is injected 13 mm downstream of the leading edge. The injection ports had a diameter of 2 mm and were inclined at 45° relative to the intake ramp (72.1° relative to the horizontal) thus giving an elliptical opening for the injectors on the intake ramp itself [2]. Five injectors were located at positions of 10, 30, 50, 70 and 90 mm along the span of the intake ramp.

Data was taken with sidewalls attached and unattached. The freestream Mach number was approximated at 7.6 with static conditions of Table 1 [2]. The fuel is injected at Mach 1 for the conditions in Table 2 [2]. A steady-state test time of approximately 1 ms was achieved and output data important to this discussion was in the form of static pressure measurements down the centreline of the intake and thrust ramp. Only a portion of the pressure along the ramp is captured by the transducer data presented in the paper. Analysis and comparison is made by normalizing the static pressure measurements against the freestream total pressure.

	Pressure (kPa)	Temp. (K)	Density (kg/m <sup>3</sup> )
<b>Walls Up</b>	2.4	270	0.03114
<b>Walls Down</b>	2.2	290	0.02636

Table 1: Freestream conditions with sidewalls attached/unattached.

	Total Press. (kPa)	Total Temp. (K)	Density (kg/m <sup>3</sup> )
<b>Walls Up, Mixing Only</b>	134	294	0.701
<b>Walls Up, Combustion</b>	138	294	0.722
<b>Walls Down, Mixing Only</b>	187	294	0.978
<b>Walls Down, Combustion</b>	185	294	0.968

Table 2: Fuel injection conditions with walls attached/unattached.

## Numerical Model

The numerical code is 3D structured, finite-volume, cell-centred solver with capability for modelling turbulent reacting flows with finite-rate kinetics. Because the nature of hydrogen storage and transportation somewhat limit its application to operational military systems, the numerical study also examined the performance of ethylene fuel using equivalent geometry and inflow conditions. For the  $H_2$  combustion a chemical kinetics mechanism with 9 species and 18 reactions was used, and the ethylene mechanism consists of 10 species and 10 reactions. All calculations were performed using a standard  $k-\omega$  turbulence model. The inviscid fluxes were evaluated using the Edwards Low Dissipation Flux Split Scheme along with a second order Kappa =  $1/3^{rd}$  MUSCL scheme. The limiter was van Leer TVD.

Due to the geometrical symmetry of the ramp, the numerical model used planes of symmetry on both sides of the ramp in the axial direction. The injection ports were modelled as squares with a cross sectional area equivalent to that of the circular feed tube of the fuel line. Although this approach did not capture 3D effects of the elliptical opening of the fuel jet, it did maintain a constant fuel mass flow rate consistent with the experiment.

The 3D mesh consisted of 2.1 million cells and contained 5 different regions beginning with an inflow region ahead of the intake ramp followed by 2 regions on both the intake and thrust surfaces. The first region captured the fuel injection 13 mm downstream of the leading edge and extended just far enough upstream to capture reattachment of the separation bubble following the fuel injection. This region was solved via an elliptical technique due to the reversed flow of the separation. The remaining regions were solved using a space marching technique which required significantly less time and resources than the elliptical solver. Cells were clustered near the walls ( $y^+ \leq 100$ ), near the injection ports, and at the apex between the intake and thrust surfaces.

Convergence was determined via norm residuals of the combined local velocity/entropy and density products. The goal was generally to achieve 4 orders of magnitude residual reduction, although in some cases the norm levelled off between 2.5 and 4.

## Discussion of Experimental/Computational Results

Figure 1 shows a comparison of CFD at the symmetry plane and the experimental results with sidewalls up and down. The measured pressure with the sidewalls-up is higher than that for sidewalls-down case due to additional compression from the sidewalls shocks. It is also the reason why the pressure data has peaks and troughs while the CFD results are relatively flat. Since the CFD method did not model sidewall effects, it is expected to follow closer the experimental data taken without sidewalls, which is confirmed in Figure 1 for air only. With the sidewalls-down, the CFD result tends to over-predict the pressure along the intake surface. This was observed in all 3 cases of air only (Figure 1), fuel injection without combustion (Figure 2), and fuel injection with combustion (Figure 3). This is attributed to air bleed over the sides of the intake ramp and edge expansion shocks after the initial shock from the leading edge. On the thrust surface the CFD results agreed reasonably well with the measured values for air only.

With the injection of the fuel (without combustion) in the sidewalls-up case, the CFD model under-predicts the ‘walls up’ experimental results (Figure 2) and over-predicts the ‘walls down’ case. The numerical predictions on the aft surface are notably lower than the measurements for the sidewalls-up arrangement. This may be attributed to further compression of the flow past the ramp apex by sidewall shocks and boundary layer effects. The oscillatory pressure behaviour along the intake ramp is evident both experimentally and in the CFD results. This

behaviour is due to a combined effect of the freestream interaction with the fuel jets, and in the sidewalls-up case, the sidewalls compression shocks. For the sidewalls-down arrangement, one might expect that the aft surface CFD results would follow the trend of under-predicting the experimental data, but the results show a nearly optimal estimation of the experiment. Since bleed over the sides is still occurring, there may be additional compression of the flow not already accounted for (ie, transient shock within the tunnel).

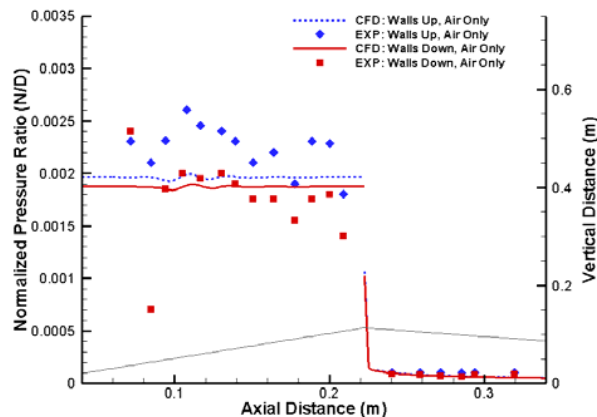


Figure 1: Experimental/computational data comparison for air flowing over an intake ramp at freestream Mach equal to 7.6.

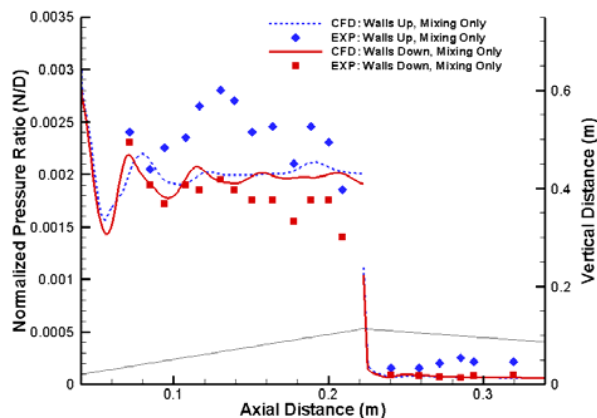


Figure 2: Experimental/computational data comparison with  $H_2$  injection into  $N_2$  (for experiment – reactions turned off in CFD).

With fuel injection and combustion, once again on the intake ramp the pressure is over-predicted for ‘walls up’ and under-predicted for ‘walls down’ for reasons mentioned previously (Figure 3). On the thrust surface the experimental results are under-predicted for both walls up and walls down. Since the margin between CFD and experimental results has increased when comparing Figures 2 and 3, it is possible that a pressure rise due to combustion is occurring on the aft surface which the numerical solution is not picking up.

Considering that the CFD model did not account for edge-bleed effects or sidewall compression, and that no error estimates are available for the measured data, it is difficult to assess the accuracy of the numerical predictions. Overall the CFD predictions capture, at least qualitatively, the flow characteristics, and may also, quantitatively, still be within the bound of

experimental uncertainty which may include, but not limited to, accurate measurement of the inflow conditions, fuel injection specifications, and pressure transducer measurement accuracy.

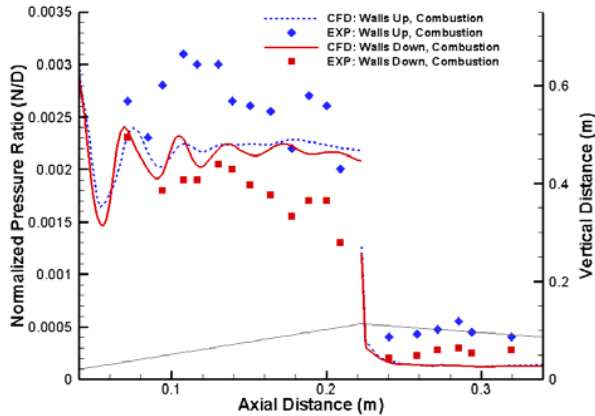


Figure 3: Experimental/computational data comparison with H<sub>2</sub> injection and combustion.

Additional attention within the experiment was given to the overall pressure profile comparison between air only, fuel injection without combustion (into a nitrogen freestream), and fuel injection with combustion. For the situation in which the sidewalls were up, these results were compared against one another to quantify the potential for drag reduction and thrust augmentation via pressure differentials on the fore and aft surfaces. The experimental approach was to take pressure data from the transducers and, using a time trace of those measurements, integrate across the surface to determine a change in pressure between the 3 cases. The numerical results for the three cases (for the ‘walls up’ freestream conditions) are presented in Figure 4. Keeping in mind the experimental results only covered a portion of the ramp area, the conclusion for the experiment was that on the intake surface, the difference between air only and mixing was practically nil, while fuel injection with combustion gave a 10% rise in the axial drag penalty. Integration of the numerical axial pressure force (for the entire ramp surface areas) on both the intake and expansion surfaces gave reasonable agreement with this conclusion.

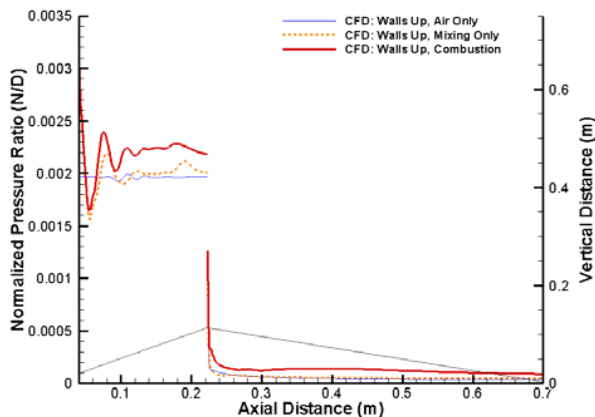


Figure 4: Computational data comparison for air only, mixing only, and mixing with combustion over an intake and thrust surface for the ‘walls up’ freestream conditions.

With mixing of the fuel (without combustion) on the intake surface increased the axial pressure force by 1.1% while combustion increased it by 9.9% (Table 3), relative to the ‘air only’ condition.

	Intake (N)	Expansion (N)	Net (N)
<b>Air Only</b>	122.9	-3.1	119.8
<b>Mixing Only</b>	124.5	-3.5	121
<b>Combustion</b>	135.1	-7.5	127.6

Table 3: Integrated axial pressure force over entire ramp surface areas.

On the aft surface the conclusions of the experiment were that addition of fuel by mixing alone increased the pressure on the thrust surface by three times (relative to either the ‘air only’ or ‘mixing only’ condition.) The numerical results indicate the axial pressure thrust increased by 2.4 times relative to the ‘air only’ condition (and 2.2 times relative to ‘mixing only’).

It can thus be concluded that the ‘infinite wing’ numerical modelling approach shows reasonably good correlation with the experimental results when comparing the three conditions of air only, fuel injection but no combustion, and fuel injection with combustion.

The unfortunate conclusion when analysing the numerical results is the increase in overall drag when introducing fuel for the given configuration. The intake pressure increase is due to compression of the freestream and additional compression due to fuel injection and combustion. Yet, once the flow expands around the apex of the surface the static pressure decreases and the flame moves further from the wall resulting in a static temperature and pressure contour as seen in Figures 5 and 6. Heat release of the reaction process also ‘freezes’ as a result of expansion around the apex. The result is a large degree of compression and penalty drag on the front surface and minimal advantageous thrust production on the aft surface. With the ‘air only’ case the net drag force is estimated at 119.8 N. Adding fuel without combustion increases the overall drag penalty 1.2 N. Combustion of the fuel then increases the drag penalty further to 127.6 N.

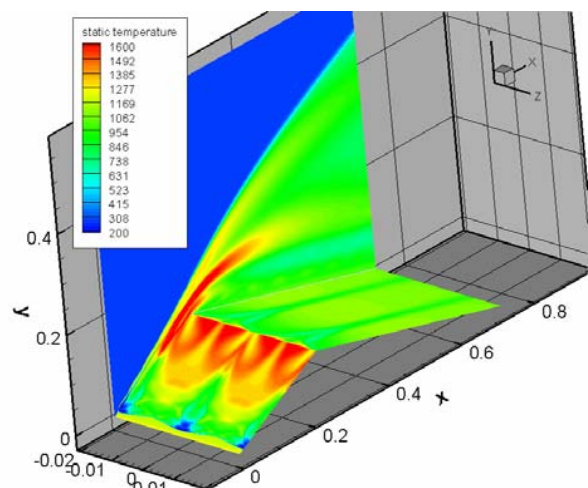


Figure 5: Contours of static temperature for H<sub>2</sub> injection with combustion.

It is evident (Figure 6) that the pressure increase on the thrust surface is occurring too far above the surface to impart a reasonable influence on the aft surface pressure of the vehicle. Further design changes to the flowpath geometry could potentially reduce this effect including location of fuel injection,

angles of ramps, method of flame stability, etc. In doing so, one must be aware of the pressure and temperature conditions after the leading-edge shock to ensure auto-ignition of the fuel.

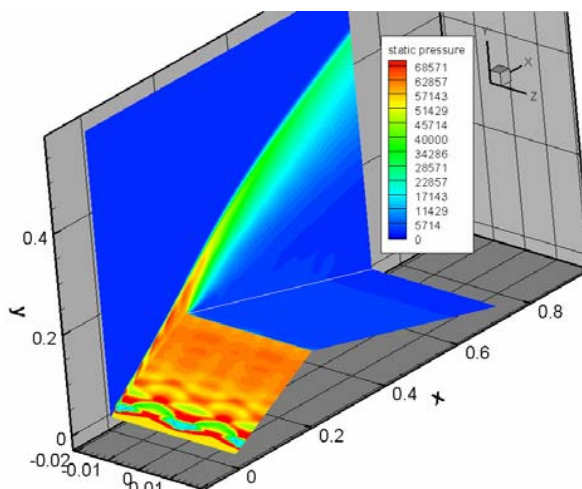


Figure 6: Contours of static pressure for H<sub>2</sub> injection with combustion.

### Discussion of Ethylene Computations

While hydrogen has been the subject of intense research and application in hypersonic vehicles and scramjets due to its ease in initiating and sustaining combustion, the logistical concerns of using such a fuel make it a less-than-desirable option. The question then turns to which hydrocarbon fuels offer reasonable alternatives. Ethylene (C<sub>2</sub>H<sub>4</sub>) is the simplest olefin hydrocarbon, which may enable a quick reaction substitute for hydrogen. A brief and basic investigation was therefore undertaken to compare the results of hydrogen (Case 0) with ethylene (Cases 1-3) using the same geometry and inflow conditions. All numerical aspects of the solver and mesh generation were left unchanged. The inflow conditions were choked for ethylene just as they were for hydrogen. The large difference in molecular weight of ethylene (for the same inflow temperature) resulted in a greatly reduced inflow velocity. In order to obtain a mass flow rate roughly equivalent to hydrogen, the density of ethylene was increased (Case 1 in Table 4). Two other cases for ethylene were also analysed which sought to equate the momentum flux and potential chemical energy release by a further increase in the fuel density (Cases 2 and 3).

Flow Parameters	H2 Case 0	C2H4 Case 1	C2H4 Case 2	C2H4 Case 3
Stoichiometric ratio	0.02913	0.068	0.068	0.068
Mass flow rate (kg/s)	0.0034	0.0026	0.0086	0.0135
Density (kg/m <sup>3</sup> )	0.805	2.553	8.362	13.040
Injection Mach (N/D)	1	1	1	1
Temperature (K)	294	294	294	294
Gas constant (J/kg-K)	4157.2	296.4	296.4	296.4
Axial velocity (m/s)	403.45	101.7	101.7	101.7
Vertical velocity (m/s)	1241.2	313	313	313
Momentum flux (N)	4.44	0.87	2.85	4.44
Heat of reaction (kJ/kg)	120,030	47,197	47,197	47,197
Heat_rxn * mass flow rate (kJ/sec)	408.1	124.6	408.1	636.3

Table 4: Physical properties of hydrogen and ethylene for fuel injection

For Case 1, using the calculated mass flow rate, the momentum flux from the injection port into the free-stream is over five times greater for hydrogen than it is for the ethylene. Contour plots of mass fraction for both hydrogen and ethylene are presented in Figures 7 and 8. The higher momentum of the hydrogen jets generate strong vortices close to the injection port, which induce enhanced mixing of the fuel with the incoming free-stream air. The ethylene jets on the other hand have weaker momentum and therefore also generate weaker turbulent mixing. Consequently, the penetration depth of the ethylene jets is short, leading to the ethylene staying attached to the intake surface.

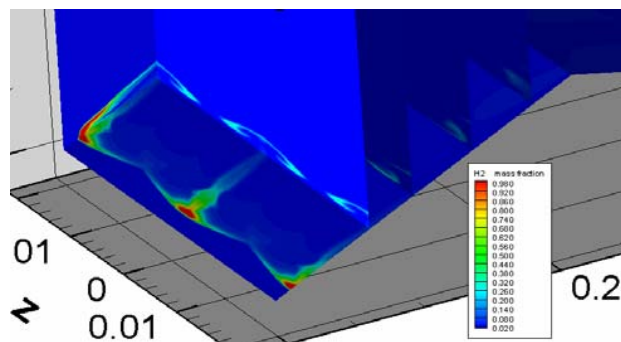


Figure 7: Contours of mass fraction of H<sub>2</sub> injection (Case 0).

In both cases a thin reaction region occurs at the stagnation point where the freestream meets the fuel jet. This results in a localised production of hydroxyl (OH) radicals and H<sub>2</sub>O (along with CO and CO<sub>2</sub> in the case of ethylene). Yet, in Case 1, the ethylene reactions are not sustained further downstream and the flame blew off completely. There is also a very small recirculation zone close to the wall in front of the injectors, but it doesn't produce any significant combustion products.

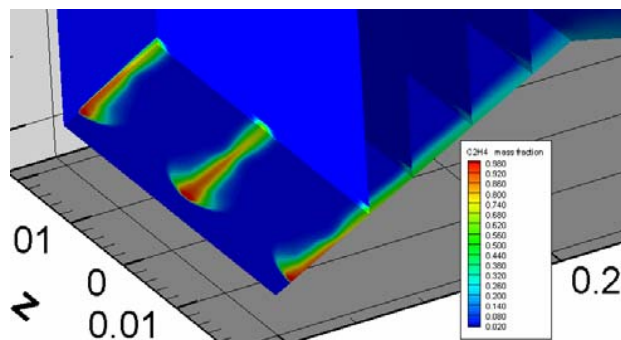


Figure 8: Contours of mass fraction of C<sub>2</sub>H<sub>4</sub> injection (Case 1).

For the H<sub>2</sub> fuel of Case 0, while autoignition commences upstream close to the injection port, the flame did not fully evolve until further downstream. Within the stable flame region, OH production increased and eventually complete combustion was achieved (see Figures 3 and 5.) For the ethylene Case 1, however, there was insufficient momentum in the fuel jet to develop this envelope region and practically no combustion product formed.

Obviously, matching the fuel mass flow rate alone for fuels with different thermochemical and physical properties does not produce equivalent results. The next step was to match the energy content of the two fuels. This was achieved by increasing the density of ethylene (Case 2), which increased the mass flow rate to match the energy content of the hydrogen (Case 0). By doing so, the momentum flux of the ethylene jet is also increased, and

for Case 2 it is only approximately 1.6 times lower than that of hydrogen. This flow configuration still did not generate sufficient mixing and/or radicals to sustain complete combustion and the flame blew off. The density of the ethylene was then increased further such that the momentum mass flux (Case 3) is the same as that for the hydrogen jet.

While the flow structure for the ethylene in Case 3 (Figure 9) appears similar to that of the hydrogen, Case 0 (Figure 7), the H<sub>2</sub>O production (Figures 10 and 11) and pressure traces (Figures 12 and 13) are different, with only partial-oxidation of ethylene occurring. There is only a minor pressure increase and variation along the thrust surface for the ethylene cases. Even for hydrogen injection the pressure increase on the thrust surface is marginal.

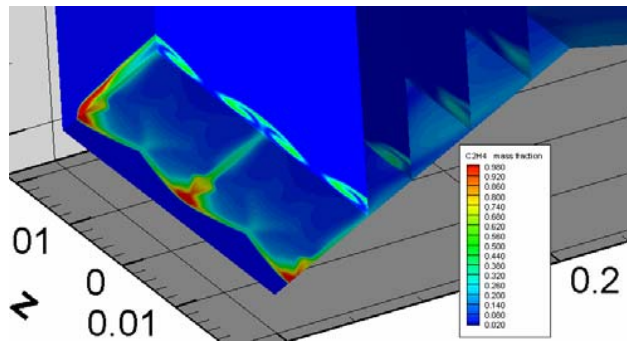


Figure 9: Contours of Ethylene mass fraction (Case 3).

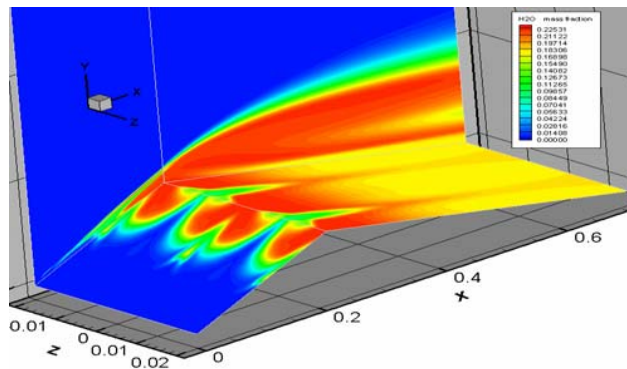


Figure 10: Contours of H<sub>2</sub>O mass fraction for H<sub>2</sub> injection (Case 0).

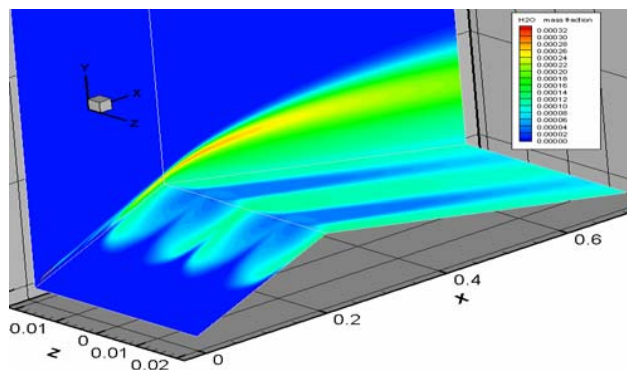


Figure 11: Contours of H<sub>2</sub>O mass fraction for C<sub>2</sub>H<sub>4</sub> injection (Case 3).

For ethylene fuel the net drag force was approximately 132 N for the three flow conditions (Cases 1, 2 and 3). For ethylene, it appears that the pressure rise on the aft surface is offset by pressure rise due to the injection and partial oxidation from the intake surface.

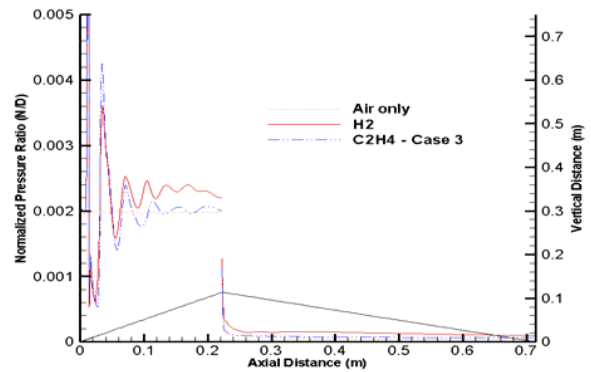


Figure 12: Comparison of static pressure to freestream total pressure ratio of hydrogen and ethylene injection (Case 3).

The results thus far indicate that matching the global flow parameters, i.e. mass flow, energy content and momentum flux of different fuels, is not sufficient to establish stable combustion. A simple possible explanation is the difference in chemical kinetics of hydrogen and ethylene. Even after a solution is fully mixed at the molecular level, a requisite time period for ambient temperature and pressure conditions is required to release the combustion energy. Using the analytical expressions for

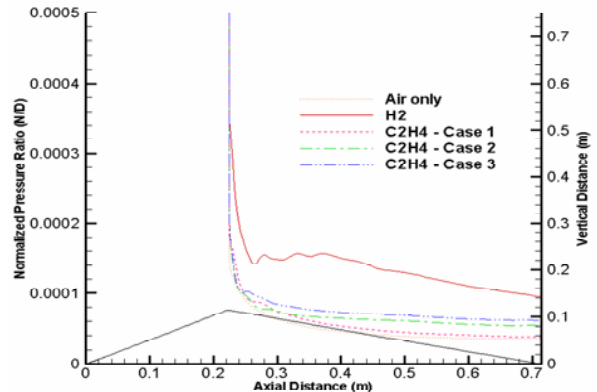


Figure 13: Comparison of normalized pressure for hydrogen and ethylene fuels over the thrust surface.

hydrogen found in reference [8] and the after-shock intake conditions measured by CFD of 1160 K and 59.2 kPa, the time required to complete 90% of energy release is on the order of  $\sim 10^{-5}$  seconds [8]. Comparable ethylene experimental results were found in Ref. [10] for the after-shock conditions and the ignition delay time (defined in that reference as the time when the pressure gradient was largest) was on the order of  $\sim 0.1$  seconds. Using a simplified free shear layer expression for the convective velocity of the mixed fuel and air streams, it is possible to approximate the distance travelled before energy release occurs. The convective velocity of the mixed streams is given in Ref. [13].

$$U_c = \frac{a_2 u_1 + a_1 u_2}{a_1 + a_2} \quad (1)$$

The variables 'a' represents the speed of sound and 'u' the velocity of the respective streams. Using the ignition delay time

(1.01e-4 sec) and the convective velocity (1649 m/s) from above, the ignition distance for the hydrogen fuel is estimated at 167 mm downstream from the injection port. This value is obviously for a simplified free shear layer flow. The current flow is much more complicated underneath the co-flowing fuel/air stream in terms of turbulent mixing induced by vortices, but at a minimum gives a rough idea of the worst case scenario for time and length required for the fuel and air to react. Tracing the H<sub>2</sub>O production for H<sub>2</sub> injection (Case 0) at various vertical distances (at the wall, 2.8 mm and 14.9 mm vertically from the wall) revealed that water production continued to rapidly increase until reaching the apex of the wall where one would expect the chemical reactions to freeze due to Prandtl-Meyer expansion (Figure 14). Under conditions where the equivalence ratio of air and hydrogen is one, the steady state hydrogen mass fraction is 0.24. At a total length of 225 mm the hydrogen mass fraction is 0.22 indicating the reaction process is nearly complete in the locations specified. The analytical result (167 mm) is shorter than the CFD result possibly because the fuel and air are not at the same temperature and requires additional downstream distance for the fuel to heat up.

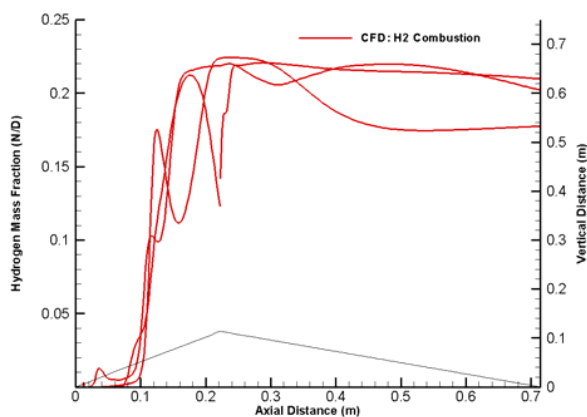


Figure 14: H<sub>2</sub>O production for H<sub>2</sub> injection (Case 0) at the wall and at vertical locations above the wall of 2.8 and 14.9 mm.

For ethylene and Case 3 conditions, the convective velocity (823 m/s) and approximated ignition delay time (1e-3 sec) give a rough estimate of 823 mm required for proper energy release. The CFD results confirm the low production of H<sub>2</sub>O and CO<sub>2</sub> at the same vertical locations above the wall as employed in the hydrogen analysis of Case 0 (Figure 15).

Flame blow-off could also be influenced by the formation, growth rate and mixing pattern within the shear layer formed between the air and the fuel streams. Using the analogy of turbulent mixing in shear layers [13], it was estimated that the convective Mach number for the hydrogen ( $M_c=0.262$ ) is similar to that of the air stream ( $M_c=0.263$ ).

$$M_c = \frac{u_1 - u_c}{a_1} \quad (2)$$

However, the convective Mach number for the ethylene in Case 3 ( $M_c=1.5$ ) is approximately 6 times larger than that of the air stream. To explore if such a large difference in the convective Mach numbers of the streams could possibly play a significant role in flame blow-off, the ethylene convective Mach number was adjusted by superficially increasing the jet velocity in the numerical initial conditions (physically could be accomplished via a diverging injection port or preheated fuel) to match that of the air ( $M_c=0.262$ ). This modification did not make any difference and the ethylene flame still blew-off. Once again

employing the simplified shear layer flow as a first-order understanding of what is happening, the formulation of Murakami & Papamouschou [12] estimates the growth rate of the thickness of the turbulent shear layer for the hydrogen/air mixture, to be approximately 10 times smaller than that for the ethylene/air mixtures. It appears that the combination of chemical fast dispersion of the mixing layer and the high convective Mach number of the ethylene, makes sustaining the chemical reactions almost impossible for the current geometry configuration.

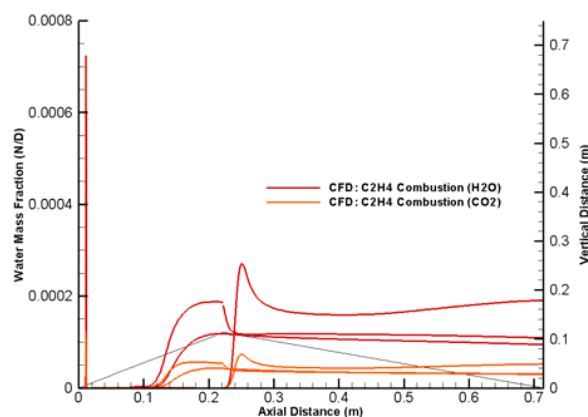


Figure 15: H<sub>2</sub>O and CO<sub>2</sub> production for C<sub>2</sub>H<sub>4</sub> injection at the wall (Case 3) and at vertical locations above the wall of 2.8 and 14.9 mm.

## Conclusions

The current analysis validated the CFD solver for external supersonic combustion of H<sub>2</sub>/air mixture. The CFD predictions generally capture the overall trend of pressure distribution, and predict the auto-ignition delay distance reasonably accurately. The relative increase in pressure between the three separate cases of air only, fuel injection without combustion, and fuel injection with combustion agree reasonably well with the experimental conclusions. Some discrepancy on the pressure trace along the aft face was noted with an additional pressure rise in the experimental results which was not seen in the numerical analysis. Several inflow conditions were modelled for ethylene/air, although none yielded a stable flame. These included equivalent mass flow, momentum flux, energy content, and convective Mach number of the ethylene jet to that of the hydrogen. It appears that the ignition-delay time is the critical parameter for sustaining chemical reaction. For all the modelled conditions, including the hydrogen flame, the drag of the vehicle actually increased once the fuel was injected into the intake ramp.

It is therefore concluded that the current geometry configuration is not suitable for external combustion of ethylene, nor is it recommended for hydrogen combustion due to significant drag increase. It is recommended to extend this study to examine surface geometry, the combustion characteristics of H<sub>2</sub>/C<sub>2</sub>H<sub>4</sub> mixtures, and exploring injection configuration, and/or a flameholder mechanism.

## Acknowledgement

The authors would like to thank Ms Samantha Coras for her assistance in setting up the numerical inflow conditions to properly match her experimental conditions. The authors also thank Dr. Nigel Smith for his valuable comments.

## References

- [1] Coras, S. & Paull, A., Experiments on External Combustion with Leading Edge Fuel-Injection in Hypersonic Flow, AIAA 2006-7981.

- [2] Coras, S. Private communication, 2007..
- [3] Stalker R.J., "Control of Hypersonic Turbulent Skin Friction by Boundary-Layer Combustion of Hydrogen", *Journal of Spacecraft and Rockets*, Vol. 42, No. 4, Jul – Aug 2005.
- [4] Billig F.S., "Supersonic Combustion Ramjet Missile", *Journal of Propulsion and Power*, Vol. 11, No. 6, 1995.
- [5] Dugger G.L., Billig F.S. and Avery W.H., "Hypersonic Propulsion Studies at APL/JHU, APL/JHU TG-405, June 1961.
- [6] Goyne C.P., Stalker R.J. & Paull A., "Hypervelocity Skin-Friction Reduction by Boundary-Layer Combustion of Hydrogen", *Journal of Spacecraft and Rockets*, Vol. 37, No. 6, Nov – Dec 2000.
- [7] Tanno H., Paull A. & Stalker R.J., "Skin-Friction Measurements in a Supersonic Combustor with Crossflow Fuel Injection", *Journal of Propulsion and Power*, Vol. 17, No. 6, Nov – Dec 2001.
- [8] Huber P.W., Schexnayder C.J. Jr, & McClinton C.R., "Criteria for Self-Ignition of Supersonic Hydrogen-Air Mixtures", NASA Technical Paper, August 1979.
- [9] Cutler, A.D. & White, J.A., An Experimental and CFD Study of a Supersonic Coaxial Jet, AIAA 2001-0143.
- [10] Varatharajan B. & Williams F.A., "Ethylene Ignition and detonation Chemistry, Part 1: Detailed Modeling and Experimental Comparison", *Journal of Propulsion and Power*, Vol. 18, No. 2, March – April 2002.
- [11] Brindle, A., Boyce, R.R., and Neely, A.J., :CFD analysis of an ethylene-fueled intake-injection shock-induced-combustion scramjet configuration", *AIAA 2005-3259, AIAA/CIRA 13<sup>th</sup> Int. Space Planes and Hypersonics Systems and Technology, 2005.*
- [12] Murakami, E. and Papamouschou D., "Eddy Convection in Coaxial Supersonic Jets", *AIAA Journal*, Vol.38, No.4, April 2000, pp. 628-638.
- [13] Shupe R.S., "Effect of Convective Mach Number in Compressible Turbulent Shear Layers", MAE 233, Turbulent Free Shear Flow, Dept of Mechanical and Aerospace Engineering, University of California, Irvine.